Quantitative Surface Plasmon Resonance Imaging: A Simple Approach to Automated Angle Scanning

ARTICLE *in* ANALYTICAL CHEMISTRY · JULY 2008

Impact Factor: 5.64 · DOI: 10.1021/ac702544q · Source: PubMed

7 AUTHORS, INCLUDING:

Rosina M Georgiadis
Boston University
43 PUBLICATIONS **3,864** CITATIONS

SEE PROFILE

Anal. Chem. **2008,** *80,* 4752–4756

Technical Notes

Quantitative Surface Plasmon Resonance Imaging: A Simple Approach to Automated Angle Scanning

Julia A. Ruemmele, Mary S. Golden, Yang Gao, Eric M. Cornelius, Mary E. Anderson, Lucian Postelnicu, and Rosina M. Georgiadis*

Department of Chemistry, Boston University, 590 Commonwealth Avenue, Boston, Massachusetts 02215

Here we present an automated angle-scanning surface plasmon resonance imaging (SPRi) instrument which provides multiplexed, quantitative reflectance data over a wide angular range. Angle-dependent artifacts, which arise from the simple optical setup, are corrected using software. This enables monitoring of significantly different surface coatings in many solvents, which would be outside the dynamic range of typical fixed-angle instruments. Operation in the visible to near-infrared range without the need for reconfiguration extends the instrument capabilities to increase sensitivity or to investigate the optical properties of surface films. This instrument provides maximum flexibility to study a wide range of systems with full exploitation of the quantitative capabilities of SPRi achieved by fitting data to the Fresnel model.

Surface plasmon resonance (SPR) spectroscopy is an optical technique known since the late 1960s[1] to be sensitive to the dielectric medium near a metal surface. Refractive index changes at the metal/dielectric interface alter the metal plasmons and hence the conditions of incident light needed to achieve optical resonance in total internal reflection geometry. The intensity of light reflected from the interface can be converted into surface coverage and monitored as a function of time to make in situ kinetic measurements of molecular binding. Label-free optical biosensors are an example of one common application of this technique.[2] SPR is ideally suited for multiplexed operation as incoherent, low-power light is used for illumination of the interface. Since the first demonstration by Rothenhausler and Knoll in 1988,[3] this multiplexed technique, known as SPR imaging (SPRi), has gained popularity for simultaneously monitoring binding events at multiple regions of interest (ROI) on patterned surfaces.[4,5]

In principle, SPRi data can provide quantitative measurements of layer thickness or surface coverage across a patterned surface in a variety of solvent environments, such as air, water, or ethanol. In practice, however, such refractive index variations, especially those associated with bulk media, can shift the SPR resonance condition out of the detection range of typical fixed-angle instruments. There are two practical approaches to compensate for this: either varying the wavelength of light at a fixed incident angle or varying the incident angle at a fixed wavelength. For the first approach to be quantitative a calibration curve must exist. In contrast, the second approach, referred to as quantitative angle scanning, simply requires an external reference angle which can be achieved with a calibrated goniometer. Additionally, angle scanning allows the user to choose the optimum angle or angles at which to monitor binding kinetics specifically for each sample. Although quantitative angle scanning is extensively used in traditional SPR (single-spot detection), its combination with imaging has only begun to be exploited.[6–8]

The largest challenge in angle-resolved SPRi is that image features change with incident angle complicating data analysis.[9] Though the beam has a fixed width, variation in the angle at which it intersects the sample surface alters the size and position of the illuminated surface area and hence changes the features captured in the SPR image. Several instrument designs avoid or minimize this problem but require specialized optical elements.[9–13] Here, we use a simple optical design and incorporate basic algorithm-based image processing to correct for the problem. Furthermore, we fully exploit the quantitative power of angle-resolved SPRi by fitting to the Fresnel model.

Finally, the instrument described here can operate at any illumination wavelength, chosen with a narrow band-pass filter, in the visible to near-infrared range without reconfiguration. The judicial selection of wavelength can improve optical coupling and sensitivity or enable the use of optical constants tabulated at

* To whom correspondence should be addressed. E-mail: rgeorgia@bu.edu. Fax: 617-353-6466.

(1) Otto, A. *Z. Phys. A: Hadrons Nucl.* **1968**, *216*, 398–410.
(2) Cooper, M. A. *Nat. Rev. Drug Discovery* **2002**, *1*, 515–528.
(3) Rothenhausler, B.; Knoll, W. *Nature* **1988**, *332*, 615–617.
(4) Brockman, J. M.; Nelson, B. P.; Corn, R. M. *Annu. Rev. Phys. Chem.* **2000**, *51*, 41–63.
(5) Campbell, C. T.; Kim, G. *Biomaterials* **2007**, *28*, 2380–2392.
(6) Wolf, L. K.; Fullenkamp, D. E.; Georgiadis, R. M. *J. Am. Chem. Soc.* **2005**, *127*, 17453–17459.
(7) Wolf, L. K.; Gao, Y.; Georgiadis, R. M. *J. Am. Chem. Soc.* **2007**, *129*, 10503–10511.
(8) Berger, C. E. H.; Kooyman, R. P. H.; Greve, J. *Rev. Sci. Instrum.* **1994**, *65*, 2829–2836.
(9) Bruijn, H. E. D.; Kooyman, R. P. H.; Greve, J. *Appl. Opt.* **1993**, *32*, 2426–2430.
(10) Shumaker-Parry, J. S.; Campbell, C. T. *Anal. Chem.* **2004**, *76*, 907–917.
(11) Johansen, K. Imaging SPR Apparatus. United States Patent 6862094, September 20, 2005.
(12) Huang, B.; Yu, F.; Zare, R. N. *Anal. Chem.* **2007**, *79*, 2979–2983.
(13) Lokate, A. M. C.; Beusink, J. B.; Besselink, G. A. J.; Pruijn, G. J. M.; Schasfoort, R. B. M. *J. Am. Chem. Soc.* **2007**, *129*, 14013–14018.

10.1021/ac702544q CCC: $40.75
Published on Web 05/14/2008

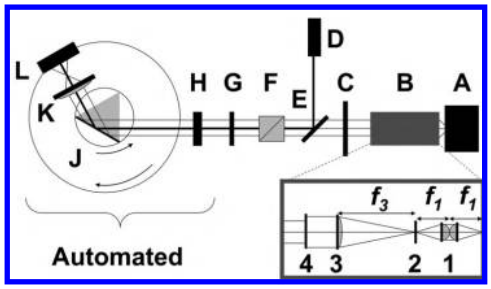

Figure 1. Instrument schematic. The letters indicate the identity of each component: A, white light source; B, collimation optics; C, wavelength filters mounted in a rotational wheel; D, HeNe laser; E, glass slide; F, polarizing cube; G, neutral density filter; H, liquid crystal variable retarder; J, prism/sample assembly; K, focus lens; L, CCD camera detector. J, K, and L are mounted on concentric rotational stages as shown. The inset shows an expanded view of the collimation optics. The numbers indicate optic identity: 1, condensing lenses; 2, pinhole; 3, collimating lens; 4, aperture. The distances indicated by the letter *f* are equal to the focal lengths of the lenses: $f_1 = 60$ mm, $f_3 = 150$ mm.

standard wavelengths. The ease of changing wavelength is especially valuable for multicolor techniques which are employed to investigate a material's optical constants.[14] The combination of all of these capabilities provides a flexible, powerful instrument for the study of surface films of various compositions ranging from biological to material science systems.

EXPERIMENTAL SECTION

Instrument Setup. A schematic of our angle-resolved SPRi instrument based on the Kretschmann configuration[15] is shown in Figure 1 and is described below. Light from a 50 W quartz tungsten halogen white light source (66172, Oriel) is collected and focused onto a 300 μm diameter pinhole (NT56-285, Edmund Optics) by two 60 mm focal length plano−convex lenses (LA1401-B, Thorlabs) as shown in the inset of Figure 1. After the pinhole, the light is collimated by a 150 mm focal length plano−convex lens (LA1002-B, Thorlabs) and the most homogeneous portion of the collimated beam is selected by a 1.3 cm diameter aperture. The wavelength of interest is isolated with the narrow band-pass filter of choice (for example, 780, 630, 580, and 540 nm; FB780-10, FB630-10, FB580-10, FB540-10, Thorlabs) from one of many mounted in a rotational wheel (FW1A, Thorlabs). The polarization is set by a broad-band polarizing beamsplitter cube (GT10-B, Thorlabs) and a liquid crystal variable retarder (LRC-200-VIS-TSC, Meadowlark, range: 450−1800 nm), for which the applied voltage needed to achieve the proper retardation is calibrated at each wavelength. At every angle, images are normalized by ratioing a p-polarized light image by an s-polarized light image.[8] These ratio images account for beam heterogeneity and time-dependent intensity fluctuations. Appropriate neutral density filters (NDxxB series, Thorlabs) are used to reduce the light intensity to within the linear response range of the charge-coupled device (CCD) detector. The light beam is directed into an SF10 equilateral prism and is internally reflected from the sample surface. The reflected image is focused by a 50 mm focal length plano−convex lens (LA1131, Thorlabs) onto a CCD camera detector (Sensys KAF0400G1, Photometrics, 81 μm^2 square pixels or Dolphin F-145B, Allied Vision Technologies, 166 μm^2 square pixels with 2 × 2 binning). The sample, CCD detector, and focus lens (which is positioned equidistant between the two) are mounted on concentric $\theta/2\theta$ goniometers (104016 and ART310-G54, Aerotech) that set the incident angle. A HeNe laser (1103P, Uniphase), which follows the beam path from the polarizing beam splitter cube to the CCD detector, is used for alignment. A specially designed mount securely holds the sample, fabricated directly on a gold-coated prism or a slide-mounted prism assembly, and the solution cell. A removable plate seals flow cells to the sample/prism assembly. The mount is positioned within 1 mm accuracy by dovetail construction and two lockable positioning plates.

At fixed angle, images can be taken as frequently as one per second to monitor fast kinetics, comparable to similar instruments in the literature.[10] The bulk refractive index range in this configuration is quite limited ($\Delta n_s \sim 0.019$, $\Delta\theta_s \sim 1.3°$, in aqueous solutions with 780 nm light where n_s is the refractive index of the bulk solvent and θ_s is the angle of the resonance minimum). In contrast, angle scanning extends the range to span $n_s = 1.00-1.40$ which allows imaging in air, water, or organic solvents. Angle-resolved data sets (known as angle scans) comprising 15−20 data points are sufficient for fitting and can be collected in approximately 2 min. Our instrument has a minimum angle increment of 0.06° and a range of 34−70°. This angular range is comparable to or better than instruments described in the literature to date[10–12] and shows a marked improvement over commercial SPRi instruments.[13]

When employing fixed angle measurements to monitor kinetics, an angle scan taken prior to binding is used to choose the appropriate fixed angle at which to monitor, either the angle of maximum contrast or the SPR minimum.[10] Another method for measuring kinetics is to collect short-range angle scans around the SPR minimum to allow optimal quantitation. In this case, the time resolution would be limited by the speed at which the CCD camera detector can capture a series of reliable images.

A graphical user interface (GUI) written in Matlab controls the hardware for data acquisition (liquid crystal variable retarder, rotational stages, and detector). Image processing in real time provides the average and standard deviation of each user-defined ROI as a function of angle or time and, when necessary, corrects the ROI pixel coordinates to account for beam walk and expansion as discussed in the Results and Discussion section. Any sequence of images can be converted into a video format to help quickly identify experimental artifacts such as bubbles or incomplete solvent mixing. The same Matlab software is used for fitting time-dependent data to a kinetic model to determine rate and equilibrium constants and for fitting angular data to the Fresnel model to determine surface coverages, as has been described in the literature.[14,16]

Sample Fabrication. SF10 glass slides (18 × 18 × 1 mm^3 polished faces 60/40 scratch-dig, Advanced Glass Industries) or SF10 equilateral prisms (L525251, Esco Products) were cleaned with standard procedures before physical vapor deposition of ~13

(14) Peterlinz, K. A.; Georgiadis, R. M. *Opt. Commun.* **1996**, *130*, 260–266.
(15) Kretschmann, E.; Raether, H. *Z. Naturforsch., A: Phys. Sci.* **1968**, *23 a*, 2135–2136.
(16) Peterlinz, K. A.; Georgiadis, R. M. *Langmuir* **1996**, *12*, 4731–4740.

Å of chromium and ~400 Å of gold.[17] Prisms and glass slides were reused by stripping the metal layers[18] and removing any remaining residue with ethanol-saturated cotton-tipped swabs.

To fabricate the patterned sample presented here a gold surface was silanized[19] and coated with SiO_x (Alfa Aesar, 36346-22) via electron beam physical vapor deposition. Six thicknesses of SiO_x were patterned on one sample surface by masking various regions during successive depositions. The SiO_x sample was silanized and coated with 10 nm citrate-stabilized gold nanoparticles (generously supplied by the Reinhard Laboratory at Boston University), drop cast from aqueous solution on the benchtop. Nanoparticles were chosen for a demonstration of a secondary deposition step because they absorb light.

Ellipsometry Measurements. Ellipsometry measurements were taken with 633 nm light (Rudolf Instruments, Auto El-II). Samples for ellipsometry were prepared as detailed above, except that microscope slides were used as a substrate and a thicker, ~1000 Å, gold film was fabricated during vapor deposition.

RESULTS AND DISCUSSION

A simple equilateral prism, which provides illumination across the entire patterned sample at a given oblique angle of incidence, also produces angle-dependent image artifacts. The first artifact, beam walk, is the lateral translation of the beam across the sample surface as illustrated in Figure 2c. As the equilateral prism rotates, the beam translation shifts the position of a feature within the beam and consequently in the captured image. Although beam walk is minimized by aligning the center of the prism on the rotation axis, its magnitude can still be significant depending on the angles of interest (see Figure 2, parts a and b). For example, an angle scan in water spanning 50−70° gives rise to approximately 2.7 mm of beam walk. A second artifact, beam expansion, is the elongation of the illuminated area of the surface along the lateral imaging dimension as shown in Figure 2e. Upon reflection from the surface, the beam condenses to its original diameter and the image features are compressed in the lateral dimension. The calculated magnitude of elongation is shown in Figure 2d. Though the illumination width changes by only ~10% over the range of an angle scan in water with 780 nm light (50−55°) the variation can be as large as ~100% over the range for 540 nm light (50−70°). Furthermore, small misalignment of the focus lens alters the projection of the beam, and hence the features, on the camera in an unpredictable way. The combined effect of these artifacts is that an ROI selected in the camera frame at one angle will not sample the same region of the surface at a different angle. This is corrected by adjusting the ROI pixel coordinates either manually, which is tedious, or through image processing.

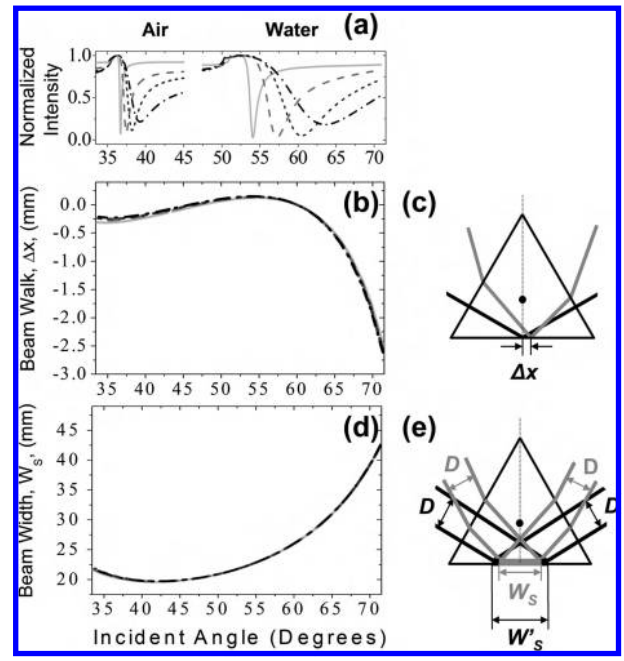

Figure 2. Illustration of two beam artifacts which result from the prism geometry. Ideal SPR curves for a gold-coated SF10 prism in air and water at multiple wavelengths are shown (a). The wavelengths are indicated by the line style (solid, 780 nm; dashed, 630 nm; dotted, 580 nm; dashed dotted, 540 nm). The resonance width decreases as the wavelength increases and also changes as a function of solvent. The width and position of the resonance determine the significance of the beam artifacts for data analysis. Part c demonstrates how the center of the beam translates across the prism sample surface (Δx) when the angle is changed. Part e illustrates that although the diameter of the beam (D) is constant, the width of the illuminated area on the sample surface (W_S or W'_S) expands as a function of incident angle resulting in condensed image features. The artifacts are exaggerated for illustration purposes. Two incident angles are depicted. The calculated magnitudes of beam walk (b) and beam expansion (d) for an SF10 equilateral prism are shown at all four wavelengths. (These calculations were based on Snell's law and simple geometry; details are provided in the Supporting Information.)

The image processing protocol for angle scans requires that the user selects a set of reference features (such as gold imperfections or fluidic cell edges) spanning the sample surface in the first frame. A normalized cross-correlation algorithm[20,21] in Matlab (normxcorr2[22]) is used to track the reference features in each subsequent frame. The accuracy and speed of processing are improved by limiting the search neighborhood, typically to within ±5 pixels, between successive frames. Successful tracking depends on appropriate selection of the reference features and the search neighborhood limits. The magnitude of adjustment for each ROI is interpolated from the reference feature tracking and depends on its location within the beam. Figure 3a shows an example of how an ROI's pixel coordinates are adjusted to monitor

(17) Cleaning was performed by submersion in hot piranha (7:3 sulfuric acid/30% hydrogen peroxide) for 10 min, rinsing with deionized water (18 MΩ), and drying with nitrogen. Metals were deposited with an e-beam evaporator at a pressure on the order of 1×10^{-6} Torr. Evaporation rates of 0.5 and 1 Å/s were used for chromium and gold, respectively. ***Safety warning***: Piranah solution is a strong oxidant which strongly reacts with organic material; caution should be used when handling the solution.

(18) Metal stripping was performed by submersion in aqua regia (3:1 hydrochloric acid/nitric acid) for 15 min, rinsing with deionized water, submersion in chromium etch (concentrated potassium ferrous cyanide and sodium hydroxide) for 5−10 min, rinsing with deionized water, and drying with nitrogen.

(19) Silanization was performed by 15 min of submersion in a solution of 5% (v/v) 3-aminopropyltrimethoxysilane, APTMS (Sigma) in methanol (Sigma), rinsing with methanol and water, and drying under nitrogen.

(20) Haralick, R. M.; Shapiro, L. G. In *Computer and Robot Vision*; Addison-Wesley, 1992; Vol. II, pp 316−317.

(21) Lewis, J. P. *Vision Interface* [Online] **1995**, 120−123. http://www.idiom.com/~zilla/Work/nvisionInterface/nip.pdf (Accessed April 23, 2008).

(22) *MatLab: Image Processing Toolbox*, 7.2.0.232 (R2006a); The MathWorks, Inc.: Natick, MA, 2006.

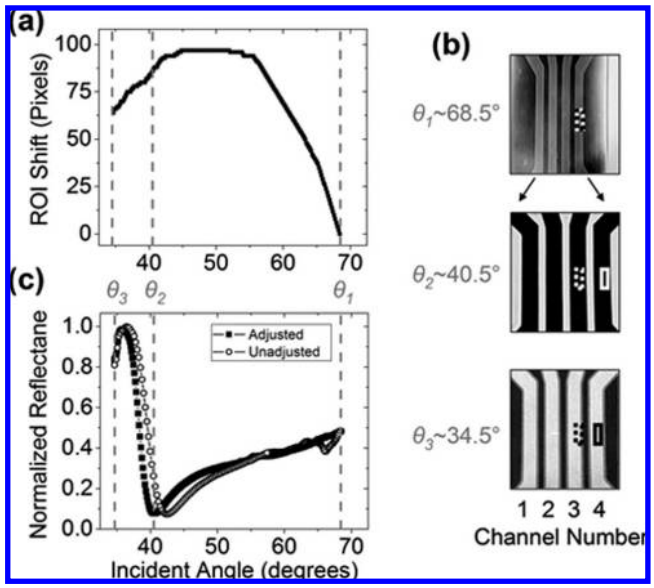

Figure 3. Demonstration of beam artifact correction. An example of the magnitude of ROI adjustment needed to continuously track a surface region is shown (a). The positions of the adjusted and unadjusted ROIs with respect to the image (solid and dashed rectangles, respectively) are shown (b) as a function of angle. The three images shown were taken at the angles indicated by vertical dotted lines in parts a and c. The reference features and the ROIs were selected at θ_1 since the features are smallest at that angle. The reference features used were the corners of the fluidic channels. The extent of change in a channel's position is a function of its location within the beam. The channels change intensity over the angle scan as the sample goes through resonance; we correspondingly change the ROI color for visibility. SPR curves obtained in air with 540 nm light are also shown (c). The solid squares are the data obtained if the ROI is adjusted to continuously monitor bare gold in channel 4; the open circles are the data obtained if the ROI is not adjusted and consequently monitors a thin layer of SiO_x in channel 3 at angles around the SPR minimum. Lines are guides to the eye.

the same surface region over a wide-angle scan. The reference features and the ROI are selected at 68.5° (θ_1) where features are the smallest (see Figure 3b). The images show a multichannel cell sample in which each channel is 1.1 mm wide. A comparison of angle scans obtained when pixel coordinates of the ROI are adjusted or not is shown in Figure 3c. The drastically different SPR curves demonstrate the consequences of beam walk and beam expansion as well as the need for such correction.

The size of the channels used for this demonstration is large compared to typical patterned surface features. We have imaged 200 μm wide surface features and estimate that our resolution is approximately 80 μm for our field of view. This instrument was designed to have a large field of view; however, a lower lateral resolution could be achieved with reconfiguration. If a larger area (or smaller pixel size) detector was used, the same field of view could be maintained while improving the lateral resolution. Recently, features as small as 2 μm have been imaged.[23] When investigating such small features, especially over a wide angular range, the effects of the beam artifacts are pronounced and the need for ROI correction is intensified. If the lateral resolution is increased, the precision of the ROI correction will increase correspondingly as both are based on the number of imaging pixels per surface area.

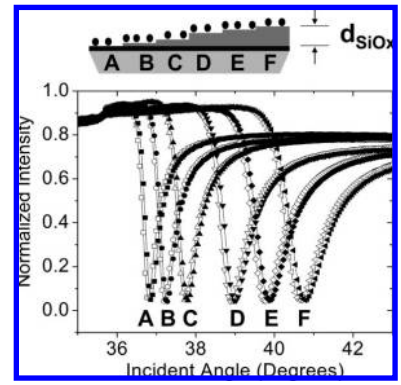

Figure 4. Wide-range angle scans. Shown are simultaneously obtained angle scans of a six-thickness SiO_x surface taken with 780 nm light in air. Open symbols indicate the angle scan of the six-thickness SiO_x sample; solid symbols indicate the angle scan of the sample coated with nanoparticles; lines are guides to the eye. The values for the SiO_x thicknesses (d_{SiOx}) determined by Fresnel fitting of the open symbol curves labeled A through F are 0, 7.5, 15, 30, 37.5, and 45 nm, respectively.

SPR curves obtained from angle scans with this instrument can be fit to the Fresnel optical model with accuracy similar to that of traditional SPR. A surface patterned with six thicknesses of SiO_x was characterized by SPRi. A single wide-range angle scan was collected to obtain full SPR curves for all regions of the sample simultaneously. Each curve was fit to the Fresnel model, assuming a dielectric constant from the literature,[24] to determine the thickness of each SiO_x region. When the results, spanning a range from 0 to 50 nm, are plotted against ellipsometry measurements of a duplicate sample a linear correlation is seen (slope of the line is 1.00 ± 0.02 and the correlation coefficient, r^2, is 0.99974) and the measurements are within ±0.46 nm of one another confirming proper operation of the instrument and the fitting protocol. We estimate the limit of detection for this system to be ~1 Å of SiO_x (3 times the standard deviation of replicate measurements) and our precision to be within 0.5% of each measured value.

The SPR curves used to determine the SiO_x thicknesses, as well as those resulting from a secondary deposition step of nanoparticles, are shown in Figure 4. The resonance positions of the SPR curves vary so significantly that a single angle could neither be used to characterize the substrate nor investigate nanoparticle deposition on all regions. This work was performed in air; however, our instrument also allows easy movement between solvents, which is especially desirable for monitoring the fabrication of biosensor surfaces. Figure 5 shows a bare gold surface imaged in air, water, and ethanol. The SPR curve changes position so drastically between solvents that it moves out of the detection range of a fixed-angle instrument. These are just two examples of studies which could not be performed efficiently without wide-angle scanning capabilities.

The shape of an SPR curve also contains information that can provide a clearer understanding of experimental results, indicate complications, or allow in-depth investigation of a sample. For

(23) Peterson, A. National Institute of Standards and Technology, Gaithersburg, MD. Personal communication, 2007.

(24) Palik, E. D. *Handbook of Optical Constants of Solids*; Academic Press, Inc.: Orlando, FL, 1985.

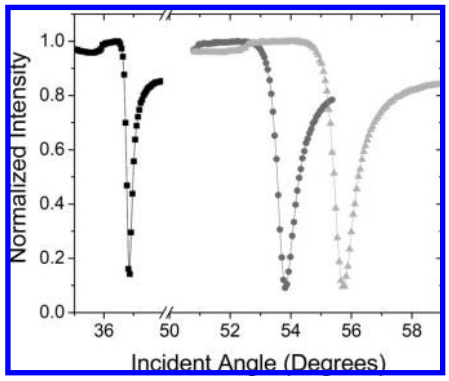

Figure 5. Demonstration of instrument operation in three solvent environments. Shown are angle scans of a bare gold surface taken with 780 nm light in air, water, and ethanol (squares, circles, and triangles, respectively). Lines are guides to the eye.

example, the shape of the SPR curve changes when incident light is on resonance with a medium's absorption band. As we have shown previously,[14] fitting angle scans of the same surface obtained with multiple wavelengths allows investigation of optical constants. We monitored the deposited nanoparticles at wavelengths on and off resonance with the their absorption band (Figure 6) and are using this technique to determine how separation from the surface effects their dielectric constants (manuscript still in preparation).[25]

CONCLUSION

We have shown that a quantitative angle-scanning SPRi instrument can be built without the need for specialized optics. Numerical correction for angular beam artifacts provides a simple and inexpensive way to facilitate the incorporation of automated angle scanning into routine analysis. The quantitative capabilities can be employed to determine optical thicknesses for a sample if the dielectric constants of the media are known. Alternatively, we can utilize multiple wavelengths of light to investigate dielectric constants and to probe behavior on and off resonance with a system being studied. The combined result is an instrument with optimum flexibility and ease of use which allows in depth investigation of any sample one wishes to study.

(25) Gao, Y.; Anderson, M. E.; Georgiadis, R. M. **2008**, Manuscript in preparation.

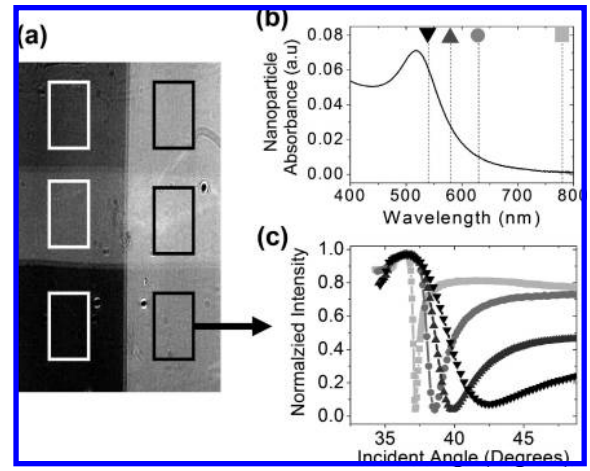

Figure 6. Demonstration of multiwavelength capabilities. An image of a six-thickness SiO_x/nanoparticle sample is shown with representative ROIs (a). The absorbance spectrum of 10 nm gold nanoparticles in water (b) and the SPR curves obtained in air from one ROI at four wavelengths (c) are provided. Points are data, and the lines are guides to the eye. The vertical lines in part b indicate the wavelengths at which we characterized the sample, and the symbols at the top of each line correspond to those of the data shown in part c (squares, 780 nm; circles, 630 nm; triangles, 580 nm; inverted triangles, 540 nm). The wavelengths chosen span on and off resonance with the nanoparticles. Similar angle scans were simultaneously collected for the other five ROIs but are not shown here for clarity.

ACKNOWLEDGMENT

This work was supported by the National Science Foundation (NSF DBI-0096731). Eric M. Cornelius was supported by the National Science Foundation (REU in Photonics, NSF EEC-0552853) and Boston University's Undergraduate Research Opportunity Program. Dr. Mary E. Anderson was supported by the Boston University Postdoctoral Faculty Fellow Program 2006−07.

SUPPORTING INFORMATION AVAILABLE

Additional information as noted in text. This material is available free of charge at http://pubs.acs.org

Received for review December 16, 2007. Accepted April 1, 2008.

AC702544Q